Available online at www.sciencedirect.com

ScienceDirect

IFAC Papers Online CONFERENCE PAPER ARCHIVE

IFAC PapersOnLine 56-2 (2023) 8420–8425

Koopman Model Predictive Control for Wind Farm Yield Optimization with Combined Thrust and Yaw Control

Antje Dittmer * **Bindu Sharan** ** **Herbert Werner** **

* *Institute of Flight Systems, German Aerospace Center, (e-mail: antje.dittmer@dlr.de)*

** *Hamburg University of Technology, Germany, Institute of Control Systems, (e-mail: bindu.sharan@tuhh.de, h.werner@tuhh.de)*

Abstract: Two novel approaches to data-driven wind farm control via Koopman model predictive control are presented, both combining thrust and yaw control for yield optimization and power reference tracking. The Koopman framework is used to build prediction models to predict wake effects of upwind on downwind turbines. This paper extends previous work by using yaw in addition to thrust control. The test case is a wind farm consisting of two turbines and wind with constant speed and direction parallel to the main axis of the farm. In closed-loop simulation, the two Koopman model predictive control designs reduce the tracking error considerably with regards to a previously published baseline controller, which used solely axial induction control. It is also demonstrated that this can be achieved with relatively small yaw angles, avoiding mechanical loads acting on turbines operating misaligned to the wind, making this a promising approach for further investigations in 3D medium and high fidelity simulation environments.

Keywords: Koopman, model predictive control, wind farm control

1. INTRODUCTION

Wind farm control is a challenging task due to aerodynamic interactions between turbines. Wake effects from upwind turbines can considerably reduce power yield from downwind turbines. Two types of wake control strategies have been demonstrated to maximize farm yield:

For wake redirection control (WRC) upstream wind turbines are misaligned from incoming flow to deflect the wake so that downstream wind turbines are less affected by wakes. This can be achieved by tilting (Cutler et al. (2021); Fleming et al. (2014, 2015)) or yawing (Cassamo and van Wingerden (2021)). WRC field test results based on yaw misalignment are reported in Fleming et al. (2019, 2020); Simley et al. (2022).

Axial induction control (AIC) varies generator torque and blade pitch angles from individual optimal settings to change the thrust by changing the axial induction factor. This decreases the power from upwind turbines, but increases the overall farm output (Bossanyi et al. (2022); Pedersen and Larsen (2020)).

In Boersma et al. (2017) the two approaches are combined to maximize power output as well as guarantee good reference tracking. In this work, two model predictive controller (MPC) designs are explored:

(1) Koopman MPC based on wind estimations from extended direct mode decomposition (EDMD): As described in Boersma et al. (2017), the upstream turbine's yaw angle for maximal power yield is calculated analytically in a first step. In a second step, the two turbines' thrust control signals are calculated via quasi linear parameter varying MPC (qLMPC) to minimize power tracking error and thrust changes, both based on estimated effective wind speeds. The effective wind speeds are derived via a Koopman model based on EDMD, identified from open loop WFSim data with the control signals as inputs and the two effective wind speeds as outputs.

(2) Koopman MPC based on farm power estimation from extended input output DMD (EIODMD): The upstream turbine's yaw angle and the thrust control signals are calculated via linear MPC to minimize tracking error, thrust and yaw changes, based directly on estimated total farm power. The total farm power is derived via an Koopman model based on EIODMD, identified with the same inputs as the EDMD model, but with total wind farm power as the output.

Koopman-based MPC for a wind farm of two turbines has been recently proposed for AIC (Cassamo and van Wingerden (2021)) and WRC (Cassamo and van Wingerden (2020)). We designed physically motivated Koopman lifting functions for real-time MPC designs, for non-adaptive (Sharan et al. (2022)) and adaptive (Dittmer et al. (2022)) AIC farm control. This work investigates the potential of including yaw control in the previously proposed algorithms that leveraged thrust changes only.

This paper is organized as follows: After an overview of EIODMD based on the Koopman framework in section 2, we provide a description of the wind farm simulation and underlying physical models in section 3. The MPC algorithms are presented in section 4, results are given in section 5, and a conclusion in section 6.

10.1016/j.ifacol.2023.10.1037

2. KOOPMAN-BASED IDENTIFICATION

The Koopman framework allows the representation of a finite dimensional nonlinear system as an infinite dimensional linear system, see for details Kaiser et al. (2020) and Proctor et al. (2018). EDMD, see Sharan et al. (2022), and EIODMD are used in this work for a finite matrix approximation of the infinite dimensional Koopman operator. Below is a short description of EIODMD. For more details as well as another application to partial differential equations, we refer to Arbabi et al. (2018).

A discrete-time nonlinear dynamical system can be given as

$$x_{k+1} = F(x_k, w_k), \quad y_k = G(x_k, w_k) \tag{1}$$

with states $x \in \mathbb{R}^{n_x}$, inputs $w \in \mathbb{R}^{n_u}$, outputs $y \in \mathbb{R}^{n_y}$ and nonlinear functions $F : \mathbb{R}^{n_x} \times \mathbb{R}^{n_u} \to \mathbb{R}^{n_x}$ and $G : \mathbb{R}^{n_x} \times \mathbb{R}^{n_u} \to \mathbb{R}^{n_y}$. Lifting functions $g : \mathbb{R}^{n_x} \to \mathbb{R}^{n_g}$ are defined as nonlinear combinations of the original states x. We define a new state $\zeta \in \mathbb{R}^{n_g}$ based on the lifting function as

$$\zeta = g(x)$$

and a finite linear approximation of the nonlinear system given in equation (1) as

$$\zeta_{k+1} = A_{\hat{K}}\zeta_k + B_{\hat{K}}w_k, \quad \hat{y}_k = C_{\hat{K}}\zeta_k + D_{\hat{K}}w_k,$$

where $\hat{y}$ is the vector of predicted output y, $A_{\hat{K}} \in \mathbb{R}^{n_g \times n_g}$ $B_{\hat{K}} \in \mathbb{R}^{n_g \times n_u}$, $C_{\hat{K}} \in \mathbb{R}^{n_y \times n_g}$, $D_{\hat{K}} \in \mathbb{R}^{n_y \times n_u}$.

For EIODMD, data of n_o samples containing the measured state, input and output vectors is collected and two data sets are assembled. One data set consists of states and inputs as

$$\mathcal{D} = \left\{ \left[x_k^T, w_k^T\right]^T \right\}_{k=1}^{n_O-1},$$

and the other data set contains the state samples shifted by one and the outputs as

$$\mathcal{D}_+ = \left\{ \left[x_{k+1}^T, y_k^T\right]^T \right\}_{k=1}^{n_O-1}.$$

The matrices $A_{\hat{K}}, B_{\hat{K}}, C_{\hat{K}}$, and $D_{\hat{K}}$ can be obtained by solving the optimization problem:

$$\min_{\hat{K}} \sum_{k=1}^{n_O-1} \left\| \begin{bmatrix} g(x_{k+1}) \\ y_k \end{bmatrix} - \hat{K} \begin{bmatrix} g(x_k) \\ w_k \end{bmatrix} \right\|_2^2 \tag{2}$$

with the Koopman matrix

$$\hat{K} = \begin{bmatrix} A_{\hat{K}} & B_{\hat{K}} \\ C_{\hat{K}} & D_{\hat{K}} \end{bmatrix} \in \mathbb{R}^{(n_g+n_y)\times(n_g+n_u)}$$

The lifting functions are applied to data from the sets $\mathcal{D}$ and $\mathcal{D}_+$ to design two matrices:

$$L_u = \begin{bmatrix} g(x_1) & \cdots & g(x_{n_O-1}) \\ w_1 & \cdots & w_{n_O-1} \end{bmatrix} \in \mathbb{R}^{(n_g+n_u)\times(n_0-1)}$$

$$L_+ = \begin{bmatrix} g(x_2) & \cdots & g(x_{n_O}) \\ y_1 & \cdots & y_{n_O-1} \end{bmatrix} \in \mathbb{R}^{(n_g+n_y)\times(n_0-1)}$$

and reformulate the optimization problem (2) as

$$\min_{\hat{K}} \left\| L_+ - \hat{K}L_u \right\|_F^2,$$

where $\|.\|_F$ denotes the Frobenius norm. The analytical solution to this linear least square problem is obtained as

$$\hat{K} = L_+ L_u^\dagger$$

where † denotes the Moore-Penrose pseudoinverse. The wind farm simulation as well as the test case used to generate data sets $\mathcal{D}$ and $\mathcal{D}_+$ are described in the next section.

3. WIND FARM SIMULATION

Open loop data as well as closed-loop results are obtained with the wind farm simulation environment WFSim, see Boersma et al. (2017). This section gives an overview of WFSim as well as the wake and wind turbine models of this simulation. The design of test cases for the Koopman system identification is also described. The code is available in Dittmer et al. (2023). Figure 1 shows a block diagram of the underlying concept for the control strategy for the wind farm of two wind turbines. The signals are

- the free-stream wind V_∞, which is kept constant at $8\,\mathrm{m\,s^{-1}}$ and aligned perpendicular to the turbines for all simulations presented in this work,
- the farm power reference P_{ref}
- the measured wind V_1 in front of turbine WT1, used as an input to the controller as in Dittmer et al. (2022)
- the thrust control signal C'_{T1} and yaw γ_1 of WT1,
- effective wind speed U_{r1}, the mean wind speed over the rotor disk of WT1,
- the power P_1 of turbine WT1,
- and the same input and output signals at turbine WT2.

The selected layout of the farm and the turbine parameters are the same as in Sharan et al. (2022). The thrust controls, controlling the energy amount harvested by a turbine, are fictitious inputs used as substitutes for generator torque and blade pitch to avoid the need for a complex turbine model. For EDMD, estimates $\tilde{U}_{ri}$ can be calculated from P_i, assuming a known power coefficient c_p.

Wake effects on the air pressure and speed are modelled

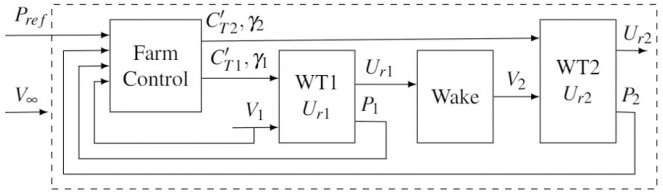

Fig. 1. Block diagram wind farm control

with 2D Navier-Stokes equations (NSE):

$$\frac{\partial \boldsymbol{u}}{\partial t} + (\boldsymbol{u}\nabla_H)\boldsymbol{u} + \nabla_H \boldsymbol{\tau}_h + \nabla_H p - \boldsymbol{f} = 0, \quad \nabla_H \boldsymbol{u} = \frac{\partial v}{\partial y}$$

where $\boldsymbol{u} = [u, v]^T$ with u and v as wind components in x and y directions respectively, partial derivative $\nabla_H = [\partial/\partial x, \partial/\partial y]^T$ and $p = p(x, y, z_h)$ as a normalized pressure with air density ρ at hub height. $\boldsymbol{\tau}_h$ is the subgrid stress tensor in horizontal direction of turbulence model and $\boldsymbol{f}$ denotes the effect of turbines on flow. Spatio-temporal discretization and detailed derivation of the 2D NSE can be found in Boersma et al. (2018).

The continuous-time wind turbine model for power and force of the i^{th} turbine in the farm is:

$$\begin{aligned} U_{ri}(\gamma_i) &= \cos(\gamma_i)\sqrt{\frac{1}{n_r}\sum_{j=1}^{n_r}(u_j^2 + v_j^2)} \\ P_i(\gamma_i, C'_{T_i}) &= 0.5\rho A_r c_P (U_{ri}(\gamma_i))^3 C'_{T_i} = C_P(U_{ri}(\gamma_i))C'_{T_i} \\ F_i(\gamma_i, C'_{T_i}) &= 0.5\rho A_r c_F (U_{ri}(\gamma_i))^2 C'_{T_i} = C_F(U_{ri}(\gamma_i))C'_{T_i} \\ \tau\dot{\hat{C}}'_{T_i} &= -\hat{C}'_{T_i} + C'_{T_i} \end{aligned} \tag{3}$$

with effective wind speed U_{ri} calculated as the mean speed of n_r blade segments, rotor area A_r, with force and power coefficient c_F and c_P and time constant τ.
As in Boersma et al. (2018), the three turbine states power P_i, force F_i, and the filtered thrust control signal $\hat{C}'_{T_i}$ are used to describe the turbine dynamics. The control inputs are the yaw γ_i and the thrust control C'_{T_i}. The functions C_F and C_P depend on U_{ri} and hence on γ_i. As in Boersma et al. (2018), the power and force derivatives are calculated as the difference between current power and force and the same states as a result of the inputs, see quation (3), with first order dynamics with time constant τ:

$$\dot{x}_{WTi} = A_{WTi}x_{WTi} + B_{WTi}(U_{ri}(\gamma_i))C'_{T_i},$$

with the state vector $x_{WTi} = [F_i \quad P_i \quad \hat{C}'_{T_i}]^T$ and the system and input matrices:

$$A_{WTi} = -\frac{1}{\tau}I^{3\times3}, B_{WTi} = \frac{1}{\tau}[C_F(U_{ri}(\gamma_i)), C_P(U_{ri}(\gamma_i)), 1]^T$$

The single turbine models above are concatenated into one wind farm model, with wind U_r at and yaw γ of all turbines:

$$\dot{x}_{WF} = A_{WF}x_{WF} + B_{WF}(U_r(\gamma))C'_{T_i}. \tag{4}$$

The qLPV system is defined by block diagonal system and input matrices $A_{WF} \in \mathbb{R}^{3n_T\times3n_T}$ and $B_{WF}(U_r(\gamma)) \in \mathbb{R}^{3n_T\times n_u}$ with turbine system and input matrices on their diagonals, n_u control inputs for the farm, and farm state $x_{WF} \in \mathbb{R}^{3n_T}$.
In past publication based on WFSim (Boersma et al. (2017); Doekemeijer et al. (2018); Sharan et al. (2022)), the thrust control signals C'_T were used for axial induction control, resulting in $n_u = n_T$ control inputs for a farm of n_T turbines. But WFSim also allows setting the yaw angle γ, which we apply in this work for wake redirection for power optimization. This would result in $2n_T$ control inputs. For this simple proof of concept with constant wind we made the decision to only change the yaw angle of the first turbine, as the optimal angle of the second turbine is perpendicular to the wind with $\gamma_2 = 0°$.
In all simulations in this paper, one sample k corresponds to one second, the WFSim default. An open loop simulation is run for $n_O = 28000$ samples for acquiring the sets $\mathcal{D}$ and $\mathcal{D}_+$. The thrust control signals C'_{T_1} and C'_{T_2} are set as noise signals, constructed from white noise with the values kept constant for 5 samples, a signal mean of 1.7, variance of 0.3 and lower and upper limit of 0.2 and 2. The yaw control signal γ_1 is changed every 4000 samples in steps of 5° from 0° to 30° and augmented with a band-limited noise signal, constructed similarly to the thrust control signals, but with zero mean and a variance of 0.5°. These signals are chosen to retrieve data at all relevant frequencies for all relevant combinations of control inputs. The yaw angle of the second turbine is fixed to $\gamma_2 = 0°$ for perfect perpendicular alignment with the wind.
The resulting WFSim simulation signals are then used to calculate two Koopman matrices, $\hat{K}_1$ from EDMD and $\hat{K}_2$ from EIODMD, as bases for the two MPC designs. The system dynamics of the identified systems are of 6^{th} order with

- lifted states of U_{ri} at both turbines, their square and cubic terms, i.e. $\zeta = [x, x^2, x^3]^T$ with $x = [U_{r1}, U_{r2}]^T$, reflecting the relationship between wind, force and power,
- inputs w_{K1} as controls C'_{T1}, C'_{T2}, and wind V_1, inputs w_{K2} as all inputs w_{K1} and additional input γ_1,
- outputs of the EDMD wind estimation model as effective wind speeds, i.e. $y_{K1} = x = [U_{r1}, U_{r2}]$
- and outputs of the EIODMD power estimation model as farm power $y_{K2} = P_T = P_1 + P_2$.

The matrix $\hat{K}_1 \in \mathbb{R}^{6\times9}$ can be split in the matrices $A_{\hat{K}1} \in \mathbb{R}^{6\times6}$ and $B_{\hat{K}1} \in \mathbb{R}^{6\times3}$. For this EDMD model, there is $C_{\hat{K}1} = [I^{2\times2}, 0^{2\times4}]$ and $D_{\hat{K}1} = 0^{2\times3}$. The values in the matrix $\hat{K}_2 \in \mathbb{R}^{7\times10}$ are reordered to find the optimal three control inputs given measured wind V_1 and a power reference, both constant over the prediction horizon. Hence, there is one additional disturbance state and three control inputs, resulting in matrices $A_{\hat{K}2} \in \mathbb{R}^{7\times7}$, $B_{\hat{K}2} \in \mathbb{R}^{7\times3}$, $C_{\hat{K}2} \in \mathbb{R}^{1\times7}$, and $D_{\hat{K}2} \in \mathbb{R}^{1\times3}$.
The qLMPC and the linear Koopman MPC that leverage $\hat{K}_1$ and $\hat{K}_2$ respectively are described in section 4.

4. CONTROLLER DESIGN

The objective of wind farm controllers is to achieve good power reference tracking with minimal changes in control inputs, as discussed in previous publications, e.g Vali et al. (2019), and our previous works, Sharan et al. (2022); Dittmer et al. (2022). We extend our previous work by including the yaw of the first turbine as an additional control input, in addition to the already previously used thrust control signals. The benefits of this will be provided in the results section 5. In this section, the cost function to be optimized is given and the two MPC designs based on the Koopman matrices $\hat{K}_1$ and $\hat{K}_2$ from section 3 are discussed.
The cost function $J(U)$ is formulated based on the trajectories of tracking error E and of input differences ΔU, the changes in control input U, for n_h sample steps of the preceding horizon

$$J(U) = E^T\boldsymbol{Q}E + \Delta U^T\boldsymbol{R}\Delta U = J_Q(U) + J_R(U) \tag{5}$$

with the weighting matrices set in this work based on the scalar weights Q and R as $\boldsymbol{Q} = QI^{n_h\times n_h}$ and $\boldsymbol{R} = R\cdot\mathrm{diag}(R_{u1}, R_{u2}, ..., R_{n_u}) \otimes I^{n_h\times n_h}$. The future error trajectory is

$$E = [E_1, E_2, \ldots, E_{n_h}]^T \in \mathbb{R}^{n_h}$$

where the power reference tracking error in time step k on farm level is calculated as $E_k = P_{ref,k} - P_{T,k}$.
The change in control inputs is calculated as

$$\Delta U = \left[U_1^T - C^T, U_2^T - U_1^T, \ldots, U_{n_h}^T - U_{n_h-1}^T\right]^T \in \mathbb{R}^{n_h n_u}$$

with the vector U_k containing all control inputs for all turbines at time step k and $C = U_0$ as the previous time step controls. For the two turbines considered and the default WFSim setting $n_h = 10$, this results in $\Delta U_{K1} \in \mathbb{R}^{20}$. Yaw γ_1 as a third control input gives $\Delta U_{K2} \in \mathbb{R}^{30}$. For both designs, the cost function summands of equation (5) can be written as

$$J_Q(U) = (P_{ref} - (\tilde{L}x_0 + \tilde{S}U))^T\boldsymbol{Q}(P_{ref} - (\tilde{L}x_0 + \tilde{S}U))$$
$$J_R(U) = \Delta U^T\boldsymbol{R}\Delta U$$

where the initial state $x_0 \in \mathbb{R}^{3n_T}$ is the state from the last sample and the matrices $\tilde{L} \in \mathbb{R}^{n_h\times3n_T}$ and $\tilde{S} \in \mathbb{R}^{n_h\times n_h n_u}$, which calculate the expected future trajectory of the farm power P_T. They are derived from the Toeplitz

matrices Λ and S, which give the expected future states for the preceding horizon trajectory. These matrices are different for the EDMD and EIODMD designs, as they are constructed from the Koopman matrices.

In the EDMD approach with $\hat{K}_1$ the qLPV farm model from equation (4) is used to calculate the power at farm level. This algorithm differs from the controller design that we presented in Sharan et al. (2022) only by setting the yaw of the first turbine to an optimal setting γ_1^* instead of $\gamma_1 = 0°$. The optimal yaw is calculated for the Gaussian wake model from Bastankhah and Porté-Agel (2016) which was used to make our results comparable to the results from Boersma et al. (2019). We refer to Sharan et al. (2022) for the calculation of the matrices $\tilde{L}_{\hat{K}1}$, $\Lambda_{\hat{K}1}$, $\tilde{S}_{\hat{K}1}$ and $S_{\hat{K}1}$, which are calculated from A_{WF} and B_{WF}as well as for a description of the qLMPC design with the estimated wind speeds as scheduling parameters.

In the EIODMD approach based on $\hat{K}_2$ the power P_T is estimated directly. The result is a linear MPC as this omits the effective wind speeds as scheduling parameters. For this second control algorithm, the stacked Toeplitz matrices $\Lambda_{\hat{K}2}$ and $S_{\hat{K}2}$ are based on the matrices $A_{\hat{K}2}$, $B_{\hat{K}2}$, $C_{\hat{K}2}$ and $D_{\hat{K}2}$ as

$$\Lambda_{K2} = \begin{bmatrix} C_{\hat{K}2}^T & (C_{\hat{K}2}A_{\hat{K}2})^T & \cdots & (C_{\hat{K}2}A_{\hat{K}2}^{n_h-1})^T \end{bmatrix}^T,$$

$$S_{K2} = \begin{bmatrix} D_{\hat{K}2} & 0 & \cdots & 0 \\ C_{\hat{K}2}B_{\hat{K}2} & D_{\hat{K}2} & \cdots & 0 \\ \vdots & \vdots & \cdots & 0 \\ C_{\hat{K}2}A_{\hat{K}2}^{n_h-2}B_{\hat{K}2} & C_{\hat{K}2}A_{\hat{K}2}^{n_h-3}B_{\hat{K}2} & \dots & D_{\hat{K}2} \end{bmatrix}.$$

For EIODMD P_T is estimated directly, so there is $\tilde{L}_{\hat{K}2} = \Lambda_{\hat{K}2}$ and $\tilde{S}_{\hat{K}2} = S_{\hat{K}2}$.

The next section presents the simulation results obtained in WFSim in open-loop and in closed-loop with an AIC MPC baseline controller and the two presented MPC controller designs.

5. RESULTS

Open-loop simulations are used to investigate the potential power increase from WRC as well as to confirm the similarity between the results from 2D NSE and the Gaussian wake model. Closed-loop simulations are used to investigate power reference tracking performance.

Open-loop WFSim simulation results are obtained for a step-sweep of the yaw angle γ_1 from 0° to 35° with consecutive increases by 5° after 500 samples. Figure 2 visualizes the simulated longitudinal wind. The WFSim simulation results are overlaid with the Gaussian wake model from Bastankhah and Porté-Agel (2016) with the centerline plotted as a blue dotted line and the far field wake expansion as a blue dashed dotted line. The match of the wake expansion at the rotor disc is reasonable. The angle of the Gaussian wake model in the far wake region is slightly smaller than the one of the 2D NSE model. However, the main area of speed deficit is nearly identical between the two models. Note that the centerline of the wake of a yawed turbine is curled in the near-wake region and hence the modelling of the centerline as a straight line in this region necessarily leads to discrepancies. This is addressed in more recent wake models like the Gaussian-Curl-Hybrid model from King et al. (2020). Nevertheless, we decided to use the Gaussian wake model for its simplicity and to be comparable to Boersma et al. (2019).

Figure 3 shows the power P_T as a function of the yaw angle γ_1 from the WFSim simulation as well as from the Gaussian wake model. The upstream turbine's power,

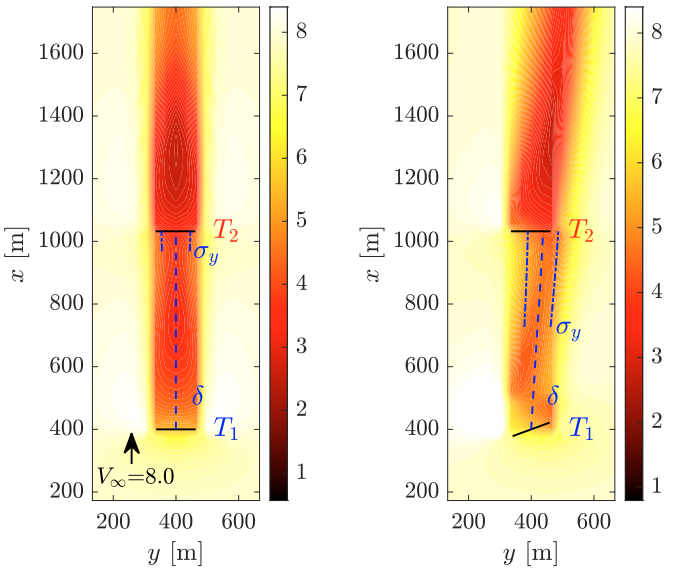

Fig. 2. WFSim wind fields, longitudinal wind for yaw γ_1 at 0° and at 20°, Gaussian wake centerline δ and expansion σ_y as blue dashed and dashed-dotted lines

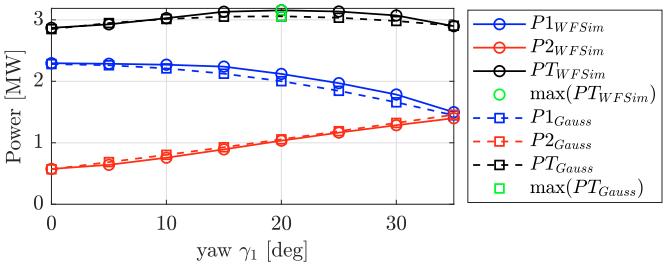

Fig. 3. Power vs. yaw angle, WFSim simulation (circles) and Gaussian wake model (squares)

plotted in blue, decreases, due to the smaller area facing the wind as well as to turbines being less efficient when yawed, see for a comparison of different models Sant and Cuschieri (2016) and for a recent field test evaluation Hulsman et al. (2022). The WFSim code operates by default with a power coefficient constant over all yaw angles, which is an unrealistic assumption. Hence, we used the values given in Sant and Cuschieri (2016) to reduce the power at higher angles to more realistic values. It can be seen that the simulation results of the first wind turbine's power still exceeds the calculations based on the Gaussian wake model for the range of 10° to 30°. However, the power curves are still relatively close. Both models predict a maximum farm yield, shown in black, around 20° yaw. The simulated power output thus confirms that the Gaussian wake model is a reasonable approximation of the 2D NSE. The farm power increase due to WRC is 10% for the 2D NSE simulation, and 6% according to the Gaussian model. Closed-loop simulations are run with the baseline MPC AIC design and the two MPC designs from section 4 using combined yaw and thrust control. The controller performance is evaluated for a power reference signal designed as a sum of a constant power and a stochastic variation

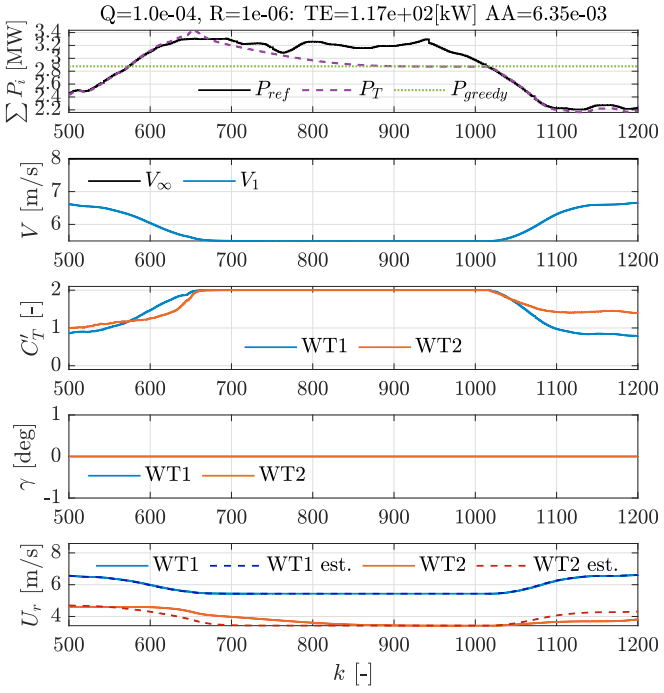

Fig. 4. Thrust control MPC based on Koopman matrix $\hat{K}_1$, yaw control signal $\gamma_1 = 0°$

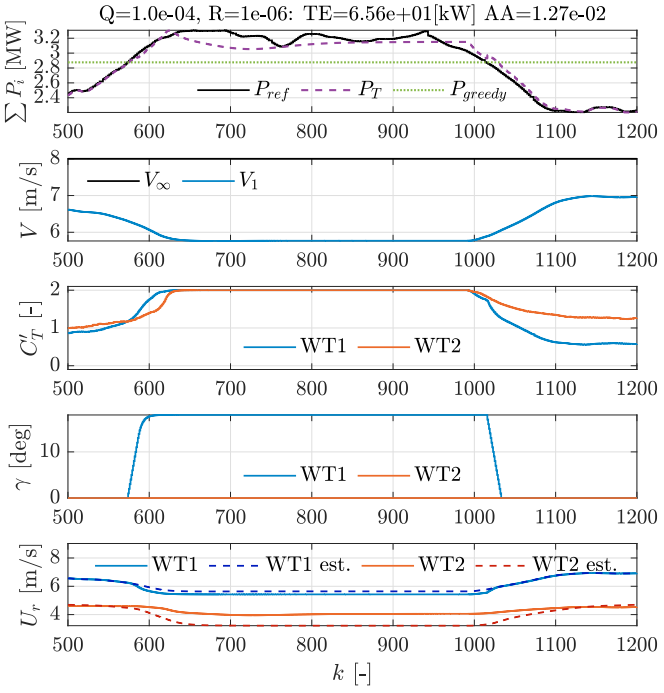

Fig. 5. Thrust control MPC based on Koopman matrix $\hat{K}_1$, yaw control $\gamma_1^* = 18°$ from Gaussian wake model

$$P_{ref,k} = (a_{const} + a_\delta \delta P_k) P_{greedy},$$

where P_{greedy} is the total farm power generated by operating both turbines with maximum thrust and the turbines aligned perpendicular to the wind. The currently used signal is adapted from a signal from Sharan et al. (2022). In that work, we set a_{const} to 0.8 and a_δ to 0.35, but kept the original values of δP. In this work, these values were reset to a_{const} to 0.9 and a_δ to 0.2. Moreover, the vector δP was resampled to change only at every second time step. The evaluation starts at sample $k = 240$ to exclude all initialization artefacts.

The closed-loop performances are quantitatively compared via the tracking error (TE) and the change in control inputs, the actuator activity (AA), the criteria used in the weighted sum from equation (5). The scalar weights Q and R are provided in the caption of figures 4, 5 and 6. The additional weighting of the three inputs is $R_{u1} = R_{u2} = 1$ for $\Delta C'_{T1}$ and $\Delta C'_{T2}$ and $R_{u3} = 0.1$ for $\Delta\gamma_{T1}$.

Figure 4 shows the closed loop performance of the baseline controller with the yaw angle constantly set to zero to align both turbines with the wind. Figure 5 displays results obtained with the first Koopman MPC control algorithm based on estimated effective wind speeds with an optimal yaw angle from the Gaussian wake model. Figure 6 displays results of the second Koopman MPC control algorithm based on estimated power outputs. The first plot shows the power yield on wind farm level, with the power reference signal depicted as a solid black line, the power yield as a dashed purple line. The power P_{greedy} is depicted as a green, dashed line. Note in figure 4 that using the thrust coefficient as the only actuator the power yield exceeds the greedy power output if the reference demands so at first, but falls back to the greedy power once the wind speed deficit that comes from setting the maximal thrust coefficient of the first turbine reaches the second wind turbine. In figure 5 the yaw is increased if

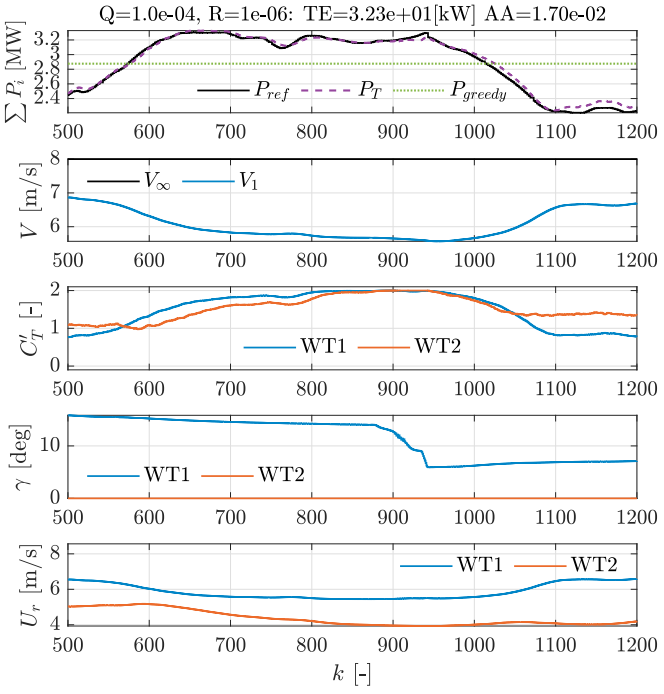

Fig. 6. Thrust and yaw control MPC based on Koopman matrix $\hat{K}_2$

the reference power exceeds greedy power, reducing the tracking error by a factor of 1.8. In figure 6 the tracking error is further reduced from 117 to 32 kW, with yaw angle included as a third control input. The actuator activity is further slightly increased, as the overall yaw rate increases. However, the control actuators of the Koopman MPC based on EIODMD result in both smaller thrust coefficients and a smaller yaw angle. This is desirable as it also decreases the forces acting on tower and blades.

6. CONCLUSION

Two Koopman MPC designs using a combination of thrust and yaw control for power yield maximization and reference tracking were presented. An open-loop simulation in WFSim showed a farm yield increase by 10% due to yaw misalignment. Closed-loop simulation with the two MPC algorithms showed that the tracking error is decreased 1.8 and 3.6 times, respectively, when including yaw control. Future work will include testing in 3D medium fidelity simulation environments that provide the possibilities to include forces and moments as objective criteria and increase the number of turbines as well as use more realistic wind test cases.

REFERENCES

Arbabi, H., Korda, M., and Mezić, I. (2018). A data-driven koopman model predictive control framework for nonlinear partial differential equations. In *2018 IEEE Conference on Decision and Control (CDC)*, 6409–6414. IEEE.

Bastankhah, M. and Porté-Agel, F. (2016). Experimental and theoretical study of wind turbine wakes in yawed conditions. *Journal of Fluid Mechanics*, 806, 506–541.

Boersma, S., Doekemeijer, B., Siniscalchi-Minna, S., and van Wingerden, J. (2019). A constrained wind farm controller providing secondary frequency regulation: An les study. *Renewable energy*, 134, 639–652.

Boersma, S., Doekemeijer, B., Vali, M., Meyers, J., and van Wingerden, J.W. (2018). A control-oriented dynamic wind farm model: Wfsim. *Wind Energy Science*, 3(1), 75–95.

Boersma, S., Doekemeijer, B.M., Gebraad, P.M., Fleming, P.A., Annoni, J., Scholbrock, A.K., Frederik, J.A., and van Wingerden, J.W. (2017). A tutorial on control-oriented modeling and control of wind farms. In *2017 American control conference (ACC)*, 1–18. IEEE.

Bossanyi, E., Ruisi, R., Larsen, G.C., and Pedersen, M.M. (2022). Axial induction control design for a field test at lillgrund wind farm. In *Journal of Physics: Conference Series*, volume 2265, 042032. IOP Publishing.

Cassamo, N. and van Wingerden, J.W. (2020). On the potential of reduced order models for wind farm control: A koopman dynamic mode decomposition approach. *Energies*, 13(24), 6513. doi:10.3390/en13246513.

Cassamo, N. and van Wingerden, J.W. (2021). Model predictive control for wake redirection in wind farms: a koopman dynamic mode decomposition approach. In *2021 American Control Conference (ACC)*, 1776–1782. IEEE.

Cutler, J.J., Stanley, A.P., Ning, A., and Thomas, J.J. (2021). Optimization of turbine tilt in a wind farm. In *AIAA Scitech 2021 Forum*, 1180.

Dittmer, A., Sharan, B., and Werner, H. (2022). Data-driven adaptive model predictive control for wind farms: A koopman-based online learning approach. In *2022 IEEE 61st Conference on Decision and Control (CDC)*, 1999–2004. IEEE.

Dittmer, A., Sharan, B., and Werner, H. (2023). Code for koopman mpc for wind farm. doi:10.5281/zenodo.7802990. URL `https://doi.org/10.5281/zenodo.7802990`.

Doekemeijer, B.M., Boersma, S., Pao, L.Y., Knudsen, T., and van Wingerden, J.W. (2018). Online model calibration for a simplified les model in pursuit of real-time closed-loop wind farm control. *Wind Energy Science*, 3(2), 749–765.

Fleming, P., Gebraad, P.M., Lee, S., van Wingerden, J.W., Johnson, K., Churchfield, M., Michalakes, J., Spalart, P., and Moriarty, P. (2015). Simulation comparison of wake mitigation control strategies for a two-turbine case. *Wind Energy*, 18(12), 2135–2143.

Fleming, P., King, J., Dykes, K., Simley, E., Roadman, J., Scholbrock, A., Murphy, P., Lundquist, J.K., Moriarty, P., Fleming, K., et al. (2019). Initial results from a field campaign of wake steering applied at a commercial wind farm–part 1. *Wind Energy Science*, 4(2), 273–285.

Fleming, P., King, J., Simley, E., Roadman, J., Scholbrock, A., Murphy, P., Lundquist, J.K., Moriarty, P., Fleming, K., van Dam, J., et al. (2020). Continued results from a field campaign of wake steering applied at a commercial wind farm–part 2. *Wind Energy Science*, 5(3), 945–958.

Fleming, P.A., Gebraad, P.M., Lee, S., van Wingerden, J.W., Johnson, K., Churchfield, M., Michalakes, J., Spalart, P., and Moriarty, P. (2014). Evaluating techniques for redirecting turbine wakes using sowfa. *Renewable Energy*, 70, 211–218.

Hulsman, P., Sucameli, C., Petrović, V., Rott, A., Gerds, A., and Kühn, M. (2022). Turbine power loss during yaw-misaligned free field tests at different atmospheric conditions. In *Journal of Physics: Conference Series*, volume 2265, 032074. IOP Publishing.

Kaiser, E., Kutz, J.N., and Brunton, S.L. (2020). Data-driven approximations of dynamical systems operators for control. In *The Koopman Operator in Systems and Control*, 197–234. Springer.

King, J., Fleming, P., King, R., Martínez-Tossas, L.A., Bay, C.J., Mudafort, R., and Simley, E. (2020). Controls-oriented model for secondary effects of wake steering. *Wind Energy Science Discussions*, 2020, 1–22.

Pedersen, M.M. and Larsen, G.C. (2020). Integrated wind farm layout and control optimization. *Wind Energy Science*, 5(4), 1551–1566.

Proctor, J.L., Brunton, S.L., and Kutz, J.N. (2018). Generalizing koopman theory to allow for inputs and control. *SIAM Journal on Applied Dynamical Systems*, 17(1), 909–930.

Sant, T. and Cuschieri, K. (2016). Comparing three aerodynamic models for predicting the thrust and power characteristics of a yawed floating wind turbine rotor. *Journal of Solar Energy Engineering*, 138(3).

Sharan, B., Dittmer, A., and Werner, H. (2022). Real-time model predictive control for wind farms: a koopman dynamic mode decomposition approach. In *2022 European Control Conference (ECC)*, 1006–1011. IEEE.

Simley, E., Debnath, M., and Fleming, P. (2022). Investigating the impact of atmospheric conditions on wake-steering performance at a commercial wind plant. In *Journal of Physics: Conference Series*, volume 2265, 032097. IOP Publishing.

Vali, M., Petrović, V., Boersma, S., van Wingerden, J.W., Pao, L.Y., and Kühn, M. (2019). Adjoint-based model predictive control for optimal energy extraction in waked wind farms. *Control Engineering Practice*, 84, 48–62.